Journal of King Saud University – Science 34 (2022) 102184

Contents lists available at ScienceDirect

Journal of King Saud University – Science

journal homepage: www.sciencedirect.com

Original article

A computational study of metal ions interaction with amyloid-β 1–42 peptide structure in hyperpyrexia: Implications for Alzheimer disease

Cosmin Stefan Mocanu [a], Laura Darie-Ion [a], Brindusa Alina Petre [a,b], Vasile Robert Gradinaru [a], Gabi Drochioiu [a,*]

[a] Faculty of Chemistry, "Al. I. Cuza" University of Iasi, 11 Carol I, Iasi 70605, Romania
[b] Center for Fundamental Research and Experimental Development in Translation Medicine, Regional Institute of Oncology, 2-4 General Henri Mathias Berthelot Str., 700483 Iasi, Romania

ARTICLE INFO

Article history:
Received 14 July 2021
Revised 8 June 2022
Accepted 13 June 2022
Available online 28 June 2022

Keywords:
In silico investigations
Hyperpyrexia
Intracranial pressure
Alzheimer's disease
Metal interactions
Conformational analysis

ABSTRACT

Given the current context of the SARS-CoV-19 pandemic, among the interfering risky factors with the Aβ peptide aggregation in the brains of Alzheimer's disease (AD) patients can be hyperpyrexia and increased intracranial pressure (ICP). According to our hypothesis on the relationship between hyperpyrexia and cognitive decline in AD, two models of Aβ peptides were used in this study: the structure of AD amyloid beta-peptide and near-atomic resolution fibril structures of the Aβ peptide. Therefore, the binding templates were constructed for Aβ peptide regions able to bind 9 different metal ions. The fragment transformation method was used for the structural comparison between Aβ chains. Molecular dynamics simulation (MDS) was applied using the Nose-Poincare-Anderson equation to generate a theoretically correct NPT (isothermal–isobaric ensemble). The smallest dissimilarities were observed in the case of Cu^{+} binding potential followed by Co^{2+}, both with similar variation. Structural changes have also occurred as a result of the dynamic simulation. All these changes suggest an aggravating factor in both hyperpyretic and AD conditions. Our findings suggest that elevated temperature and increased intracranial pressure rise the effect of peptide aggregation, by converting α-helix motif to β-sheet and random coil conformation, which are related to the formation of senile plaques in AD brains.

1. Introduction

Alzheimer's disease (AD) is a frequent neurodegenerative disease in the elderly and the most common cause of dementia, characterized by progressive cognitive deterioration. Incidence of AD continues to rise worldwide, becoming a major health challenge in the 21st century, expressed in both the medical and financial fields (Fan et al., 2020).

The neuropathological hallmarks of AD include an increase in amyloid plaques and cerebral amyloid formation, neurofibrillary tangles and glial responses, as well as neuronal and synaptic loss (Serrano-Pozo et al., 2011). According to the Chicago Health and Aging Project study, about 700,000 people with age 65 and older in the US will have AD when they die in 2020 (Weuve et al., 2014). A similar report published by Alzheimer Europe shows that the number of people with dementia in Europe is likely to double by 2050, increasing from almost 9 million to more than 18 million in the wider European region (Alzheimer Europe, 2020). Although some older adults with AD die from causes unrelated to the disease, many of them die from Alzheimer's disease or from conditions where this neurodegeneration was a contributing cause of death, such as pneumonia (Alzheimer's Association, 2020). Among the numerous hypotheses that describe progression and development of AD, the amyloid one is related to the involvement of various forms of Aβ peptides in damage to neuronal and cognitive functionality (Vijayan and Chandra, 2020). The Aβ peptides (Aβ 1–40 and 1–42) are generated as a result of abnormal APP cleavage assisted by β- and γ-secretase (Tambini et al., 2020). These peptides undergo to soluble oligomers that can exist in several conformations, which can aggregate in toxic fibrils and plaques species

* Corresponding author.
E-mail addresses: cosmin.stefan.m@gmail.com (C.S. Mocanu), laura.ion@uaic.ro (L. Darie-Ion), brindusa.petre@uaic.ro (B.A. Petre), robert.gradinaru@uaic.ro (V.R. Gradinaru), gabidr@uaic.ro (G. Drochioiu).
Peer review under responsibility of King Saud University.

Production and hosting by Elsevier

https://doi.org/10.1016/j.jksus.2022.102184

(Guo et al., 2020). Furthermore, in the presence of small molecular catalysts, some species of oligomers and end-products of Aβ peptides have been shown to convert to complete amyloid fibrils (Bieschke et al., 2012).

Besides, the interaction of Aβ peptides with metal ions such as copper, zinc, iron, manganese or nickel has been shown to contribute to neuronal damage (Sciacca et al., 2020). Moreover, copper and zinc ions have been demonstrated to modulate amyloid-β aggregation along different metabolic routes (Faller et al, 2013). In addition, the amyloid-copper fibril seeds have also been shown to initiate aggregation in non-copper solutions of Aβ (Sarell et al., 2010; Pedersen et al., 2011). Also, in the case of AD, copper supplies the neurotoxicity of the related peptides, disturbing the normal exchange of the metal ion involved in the binding (Huang et al., 1999). The accumulation of intracellular toxic aggregates, with the loss of soluble Tau protein responsible for the stabilization of microtubules in neurons, can synergistically lead to compromised brain survival, (Mocanu and Drochioiu, 2021). However, the homeostasis of metal ions, such as iron, copper and zinc in the brain is crucial for maintaining normal physiological functions. Nevertheless, numerous studies have shown that the imbalance of these metal ions in the brain is closely linked to the onset and progression of Alzheimer's disease (Wang et al., 2020). In addition, metal ion concentrations higher than physiological conditions were reported in the brain parenchyma and separated from amyloid plaques (Markesbury and Lovell, 2007). Therefore, it is important to understand the phenomena underlying the interaction between metal ions and Aβ peptides and their correlation with the aggregation process to develop new treatment therapies.

Moreover, risky factors that can interfere with the Aβ peptide aggregation in AD brains could be caused by hyperpyrexia, an elevation of body temperature above 41.0 °C. As already reported, hyperpyrexia is a predominant symptom in severe COVID-19 pathophysiology, bacterial infections, inflammatory conditions or heat exhaustion (Czepiel et al., 2020; Singhal et al., 2020; Noa et al., 2020). Body temperature affects cerebral hemodynamics and also increases cerebral blood flow velocity and intracranial pressure (Stretti et al., 2014). Amyloid-beta fibrils are generated as a result of β-sheets structures which are stacking in a parallel or antiparallel form, perpendicular to the fibril axis and held by hydrogen bonds parallel to the fibril axis (Luhrs et al., 2005; Makin et al., 2005).Phenylalanine residues and π-π stacking interactions seem to play an important role in the aggregation or self-assembly of various peptides, such as amyloid-beta $A\beta_{(1-42)}$ (Liu et al., 2021; Mocanu et al., 2022). Respiratory failure is commonly expressed in these patients, due to a decrease of oxygen level in the body. When oxygen levels drop in the circulatory system, blood pressure automatically rises, changing intracranial pressure and body temperature (Allahdadi et al., 2005). Additionally, cerebral hypoxia can lead to a poorer oxygenation of the neurons and hence, their physiological function becomes impaired. This can have a direct implication in the development of senile plaques, due to a weaker cerebral regeneration (Mukandala et al., 2016).

Therefore, it is necessary to analyze how the aggregation processes of Aβ peptides are influenced by the action of extrinsic factors induced by hyperpyrexia to provide an overview of both, thermal and osmotic impact on AD patients. In addition, experimental investigations of transition metal ions linked to amyloid-beta monomers and oligomers pose challenges due to the disordered structure of Aβ, its fast aggregation, as well as solvent and paramagnetic effects (Strodel and Coskuner-Weber, 2019; Lupaescu et al., 2021).

According to our hypothesis in which hyperpyrexia could affect the process of metal- $A\beta_{(1-42)}$ interaction, we resorted to a theoretical comparative *in silico* analysis with the purpose to investigate the structural changes in the shape of the monomer $A\beta_{(1-42)}$ and fibrils generated by $A\beta_{(1-42)}$ in the presence of various metal ions, such as Cu^{+}, Cu^{2+}, Fe^{2+}. Fe^{3+}, Mn^{2+}, Mg^{2+}, Ni^{2+} and Zn^{2+}. The analysis was based on the conformational differences between these molecular species, under normal physiological conditions of 37.0 °C and 11 mmHg and specific to hyperpyrexia conditions (up to 41.0 °C and 20 mmHg) (Ghajar, 2000).

These characteristics can provide theoretical valuable information regarding the underlying processes that occur in patients infected with hyperpyrexia under AD. Moreover, this paper highlights the first *in silico* framework for the analysis of the effect of thermal and osmotic impact on neurodegenerative processes.

2. Materials and methods

The Aβ peptides were constructed using Protein Data Bank (PDB) in Molecular Operating Environment software (MOE) with appropriate residue protonation state at physiological pH (Molecular Operating Environment (MOE), 2017). For this study, two models of Aβ peptides were used, the solution structure of the amyloid-β peptide (1–42) (1IYT; denoted $A\beta_{(1-42)}$) and near-atomic resolution fibril structures of the same peptide by cryo-EM with 9 chains of $A\beta_{(1-42)}$ (5OQV; denoted $A\beta_{(1-42)}F$) (Crescenzi et al., 2002; Gremer et al., 2017). Binding templates have been constructed for regions that could bind nine selected metal ions (Cu^{+}, Cu^{2+}, Fe^{2+}, Fe^{3+}, Mn^{2+}, Mg^{2+}, Ni^{2+} and Zn^{2+}). The templates include residues at 3.5 Å from the metal ion according to the fragment transformation method developed by Lin et al. (Lin et al., 2016; Lu et al., 2012), which was used for structural comparison between Aβ chains. Each residue of the query peptide was assigned a binding score, which is composed of the sequence and structure conservation measures. The fragment transformation method was used to align query peptide chain and metal-binding site. By this method, the query peptide was aligned with the metal-binding templates and then each cluster was scored according to its sequence and structure similarity. The BLOSUM62 substitution matrix was used to calculate the sequence similarity, and the root-mean-square deviation of the C_{α} atoms of the alignments was applied to evaluate the structure similarity (Lin et al., 2016).

The peptide-metal complex was exposed to a MMFF94x Hamiltonian force field potential energy in MOE to configure its parameters and to manage restraint forces applied to the atoms (Halgren, 1996). The energy minimizes application calculates atomic coordinates that are at local minima of a molecular energy function. For this purpose, the gradient was set at 0.05, when the gradient of root mean square falls below that specified value. The root mean square gradient was the norm of the gradient times the square root of the number of unfixed atoms. Water-solvent molecules were also added to the system, positioned in a rectangular arrangement around the peptide-metal complex.

The simulation of molecular dynamics was applied using Nose-Poincare-Anderson equation to generate a theoretically correct NPT ensemble (Bond et al., 1999; Sturgeon and Laird, 2000). The temperature response used to enforce constant temperature was set at 0.2 picoseconds (ps), and the pressure response used to enforce constant pressure at 5 ps. In the first molecular dynamics ensemble, to analyze the conformational and structural changes that occurred to the peptide-metal complex under physiological conditions, a heat time of 200 ps at 310.15 K (37.0 °C) and 1.466 kPa (11 mmHg, the mean value for normal intracranial pressure) was applied. For the second state, the temperature was set to 314.15 K (41.0 °C) and 2.666 kPa (20 mmHg, the mean value for ICP) for 200 ps. The system was monitored at the time step of 0.0005 ps.

3. Results

3.1. The binding potential

First, we studied the binding of the nine metal ions (Cu^{+}, Cu^{2+}, Fe^{2+}, Fe^{3+}, Mn^{2+}, Mg^{2+}, Ni^{2+} and Zn^{2+}) to $A\beta_{(1-42)}$ peptide and 9 chain $A\beta_{(1-42)}$ fibrils ($A\beta_{(1-42)}F$). Both the $A\beta_{(1-42)}$ monomer and the fibrils were taken from the PDB database as validated structures and analyzed using the fragmentation method described in Section 2 (Fig. 1).

As can be seen from Fig. 1a, in the case of the $A\beta_{(1-42)}$ monomer peptide, the binding potential is predominantly expressed in sequence 1–16, while this index tends to be much lower in the rest of the Aβ structure. This is most likely due to the amino acid residues such as His, Ser or Asp at Aβ N-terminal, which contain nitrogen or oxygen atoms that play an electron donors role in the ligand-receptor interactions.

On the other hand, in the case of $A\beta_{(1-42)}F$, the binding potential of the metal ions increases even in the region 17–42, which suggests that, compared to the monomer Aβ, metal ions tend to bind to the entire structure of Aβ peptides in fibrils. Hence, these ions tend to bind much easier because $A\beta_{(1-42)}F$ has a much larger binding surface and stability. An alternative explanation involves the inhibition of the α-helix structure in $A\beta_{(1-42)}F$ to the advantage of the β-sheet and random coil pattern, the helix structure prevents the formation of coordinative bonds. Von Bergen and coworkers have demonstrated that the assembly of Tau protein into AD paired helical filaments depends on a local sequence motif (Von Bergen et al., 2000).

Furthermore, by comparing the potential binding plots between $A\beta_{(1-42)}$ and $A\beta_{(1-42)}F$ significant differences regarding metal ions interaction were noticed. These differences can be analyzed by decreasing the binding potential of each metal in $A\beta_{(1-42)}$ with the binding potential of the same metal for each chain in $A\beta_{(1-42)}F$.

According to these results (Fig. 2), the smallest dissimilarities can be noticed in the case of Cu^{+} binding potential followed by Co^{2+}, both with similar variation. On the other hand, major differences were observed between the binding of Mn^{2+}, Ni^{2+}, Mg^{2+} and Fe^{2+}. Cu^{2+} and Zn^{2+} ions showed the same deviation from the difference, whereas the most notable variation was observed in the 1–16 Aβ fragment for Fe^{3+}.

Therefore, by analyzing these findings, we selected Cu^{+} ion in our investigation, because it provides the most constant binding potential regarding the structure of $A\beta_{(1-42)}$ or $A\beta_{(1-42)}F$.

3.2. Conformational and structural analysis

The $A\beta_{(1-42)}$-Cu^{+} complex was studied using the molecular dynamics protocol in order to analyze the influence of the metal ion under the imposed dynamic conditions. The conformations resulted regarding the $A\beta_{(1-42)}$-Cu^{+} at 37 °C (11 mmHg) and 41 °C (20 mmHg), as well as the Cu^{+} coordination pattern at the peptide binding site can be observed in Fig. 3.

According to Fig. 3a, Fig. 3b and Fig. 3c, noteworthy modifications can be noticed regarding the structure of the $A\beta_{(1-42)}$ peptide under the influence of the copper ion, as well as under the influence of temperature and pressure. An improved breakdown of these structures according to their conformation can be seen in Fig. 4. Thus, the specific conditions of hyperpyrexia inhibit the α-helix motif to the advantage of the β-sheet for the Glu^{11}-Gln^{15} sequence in the case of normal physiological conditions (37 °C, 11 mmHg) and for the Glu^{11}-Phe^{20} and Gly^{25}-Ile^{31} sequence in the case of high fever (up to 41 °C and 20 mmHg). This β-sheet motif and consequently, the random coil structure, increases the aggregation processes by promoting the formation of new intermolecular hydrogen bonds (Sturgeon and Laird, 2000). This suggests that an elevated temperature and ICP intensify the peptides aggregation processes at the cortical level, with direct consequences on the AD pathophysiological morphology. In addition, as can be seen from Fig. 3d (2f) and Fig. 3e (3 g), after applying the dynamic conditions the coordination model of Cu^{+} at the binding site was changed.

According to these data (Table 1), the coordination bonds length between the metal ion and the amino acid involved in the binding process are modified. In the case of Cu^{+}-Glu^{11} at 37 °C the bond length was 1.74 Å while at 41 °C was 1.72 Å. For Cu^{+}-Tyr^{10}, the length modifies from 2.18 Å to 2.22 Å. This suggests that even for 200 ps simulation, the bond between metal and Glu^{11} becomes stronger (Fig. 3g), while the Cu^{+}-Tyr^{10} bond turns out to be weaker. However, the benzene ring of Tyr appears to interfere with its backbone through π-cation interactions (Fig. 3f and Fig. 3g). The distance between Cu^{+} and the benzene ring changes from 3.00 to 2.97, which indicates that the benzene ring acts as a stabilizer for the Cu^{+}-Glu^{11} complex.

Subsequently, the metal ion binding and its influence on the Aβ fibrils were analyzed. The resulting conformations in the case of $A\beta_{(1-42)}F$-Cu^{+} at 37 °C (11 mmHg) and 41 °C (20 mmHg), as well as the Cu^{+} ion coordination pattern at the peptide binding site can be observed in Fig. 5.

Fig. 5 shows significant differences between the interactions of the Cu^{+} ion with each peptide chain within $A\beta_{(1-42)}F$. In the case of $A\beta_{(1-42)}$, the major modification occurred in the structure conformation due to inhibition of the α-helix to the advantage of the β-sheet motif, whereas in the case of Aβ-amyloid fibrils, the modifications were linked to the lack of α-helix motif in the chains structure (Fig. 5a). The noteworthy changes can be analyzed in terms of binding sites and interaction between the Cu^{+} and the corresponding amino acid (Fig. 5b). The results regarding the bond lengths of the $A\beta_{(1-42)}F$-Cu^{+} complex for each chain can be seen in Table 1.

According to Table 1, the amino acid most often engaged in Cu^{+}-binding processes was His(N), followed by Tyr, His(O) and Val. From the analysis of these lengths, Tyr and Val tend to dissociate from Cu^{+} at higher temperature and pressure, while His(N), His (O), Glu and Gln strengthen the coordination bond. This suggests that amyloid peptide fragments with multiple residues of His (through the nitrogen atom), Glu and Gln are better ligand-receptor for binding copper ions.

3.3. Ramachandran analysis

A better understanding of Aβ peptides conformations can be achieved by analyzing the Psi and Phi angles, using the Ramachandran plot. (Fig. 6).

According to Fig. 6a, $A\beta_{(1-42)}$ monomer displayed a right-handed α-helix conformation with an extension in parallel β-sheet (left quadrant), while the most of the angles values are in anti-parallel β-sheet in the case of $A\beta_{(1-42)}F$ (Fig. 6b), parallel β-sheet and collagen helix area (upper left quadrant), with a few in left-handed α-helix (upper right quadrant) and right-handed α-helix (lower left quadrant). Following the application of dynamic conditions, no significant structural differences were observed in the case of $A\beta_{(1-42)}$ in both physiological and hyperpyretic conditions. However, a larger dispersion of the angle values to the upper left quadrant specific to the parallel β-sheet (Fig. 6d and Fig. 6e) was observed. These data are well correlated with those obtained by conformational studies presented in *Section 3.2*.

In the case of $A\beta_{(1-42)}F$ structure, the same buildup characteristics were noticed in the β-sheet area in both circumstances (Fig. 6f and Fig. 6g). However, the difference was observed in the lower left quadrant (the right-handed α-helix area). Following molecular dynamics condition, at higher temperature and pressure, the angle

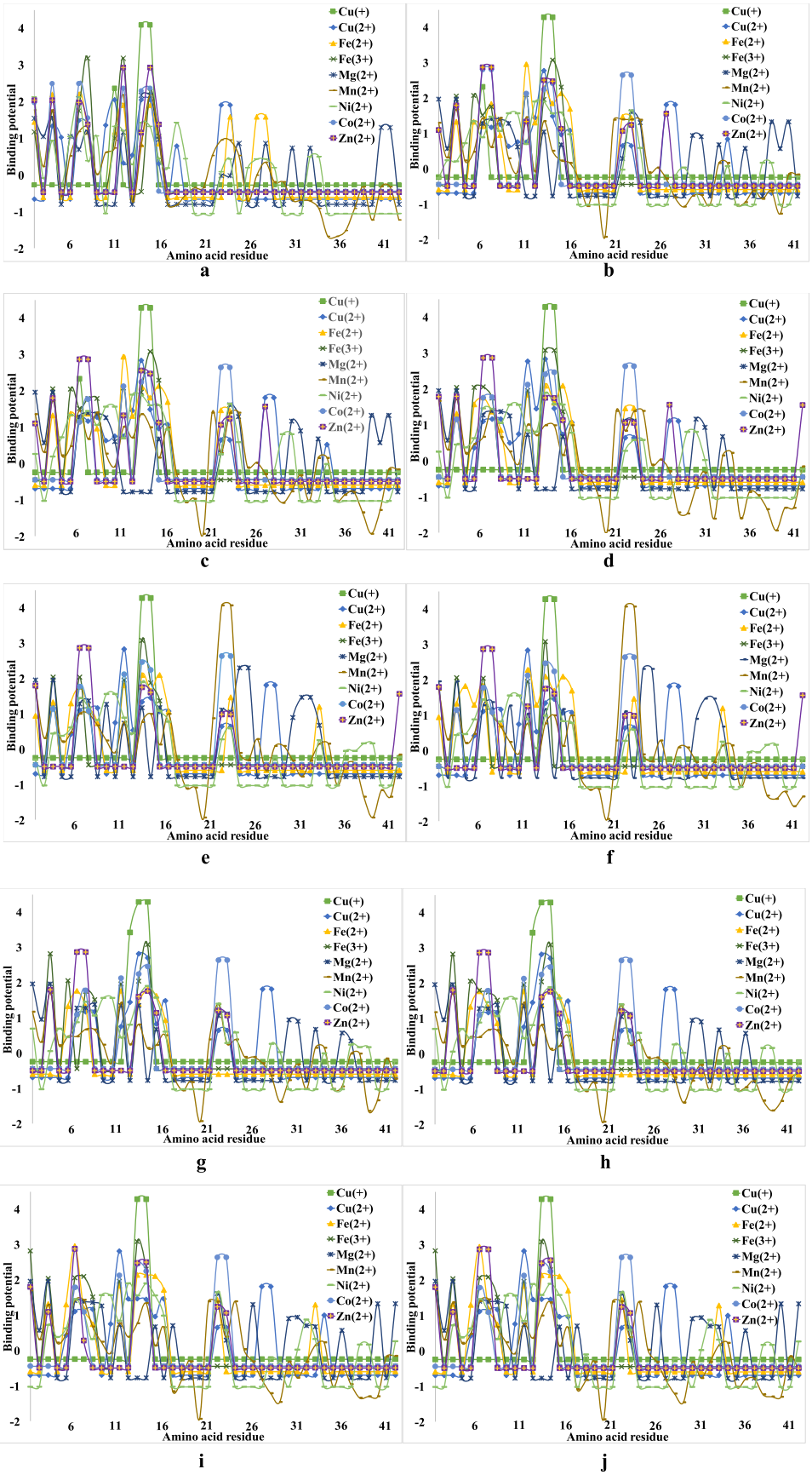

Fig. 1. The binding potential of the metal ions involved in the Aβ peptide complexation process, where: (**a**) – $A\beta_{(1-42)}$; (**b**) – $A\beta_{(1-42)}$F Chain 1; (**c**) – $A\beta_{(1-42)}$F Chain 2; (**d**) – $A\beta_{(1-42)}$F Chain 3; (**e**) – $A\beta_{(1-42)}$F Chain 4; (**f**) – $A\beta_{(1-42)}$F Chain 5; (**g**) – $A\beta_{(1-42)}$F Chain 6;(**h**) – $A\beta_{(1-42)}$F Chain 7; (**i**) – $A\beta_{(1-42)}$F Chain 8 and (**j**) – $A\beta_{(1-42)}$F Chain 9.

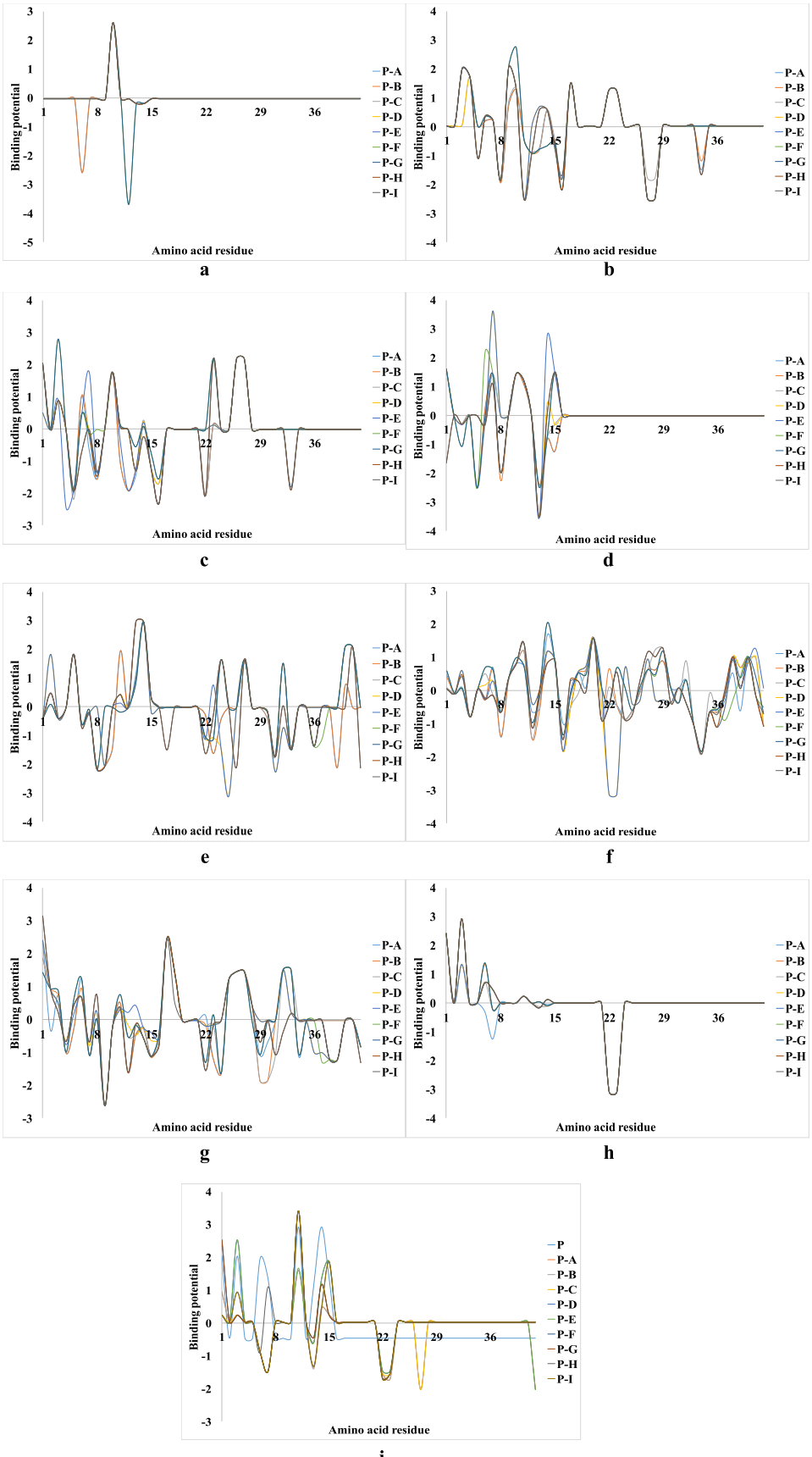

Fig. 2. The binding potential differences o of each metal ion from $A\beta_{(1-42)}$ with the binding potential of the same metal for each chain from $A\beta_{(1-42)}F$, where: P – the chain of the $A\beta_{(1-42)}$ and A, B, C, D, E, F, G, H and I represent the 9 fibrillar chains of $A\beta_{(1-42)}F$; (**a**) Cu^{+}, (**b**) Cu^{2+}, (**c**) Fe^{2+}, (**d**) Fe^{3+}, (**e**) Mg^{2+}, (**f**) Mn^{2+}, (**g**) Ni^{2+}, (**h**) Co^{2+} and (**i**) Zn^{2+}.

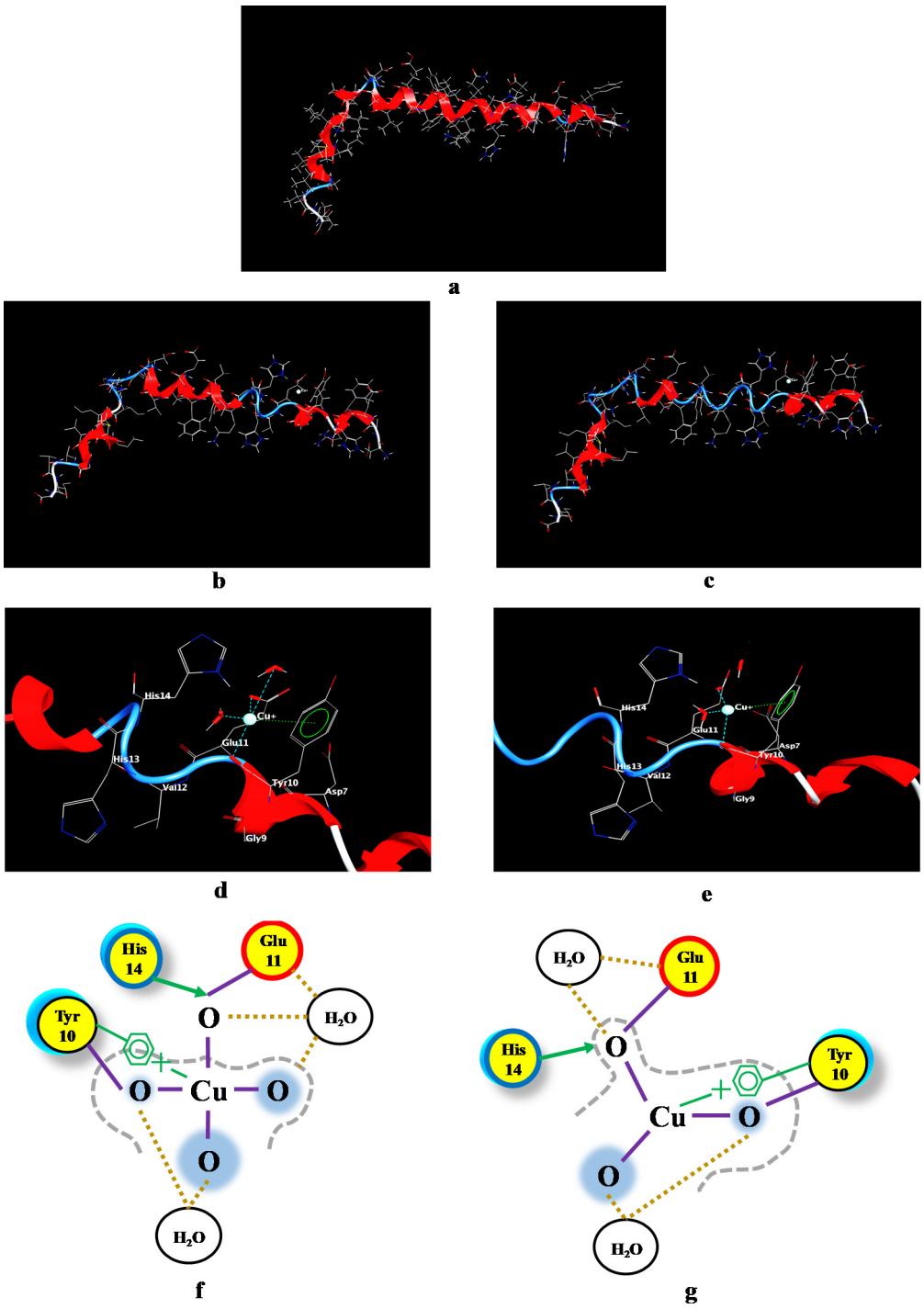

Fig. 3. The $A\beta_{(1\text{-}42)}$-Cu^{+} complex conformation resulted following the application of molecular dynamics under the conditions imposed (temperature and pressure), where: (**a**) $A\beta_{(1\text{-}42)}$ peptide structure; (**b**) The structure of $A\beta_{(1\text{-}42)}$-Cu^{+} complex at 37 °C and 11 mmHg; (**c**) The structure of $A\beta_{(1\text{-}42)}$-Cu^{+} complex at 41 °C and 20 mmHg; (**d**) $A\beta_{(1\text{-}42)}$-Cu^{+} binding site at 37 °C and 11 mmHg; (**e**) $A\beta_{(1\text{-}42)}$-Cu^{+} binding site at 41 °C and 20 mmHg; (**f**) Coordination pattern of the Cu^{+}-amino acids at 37 °C (11 mmHg) and (**g**) Coordination pattern of the Cu^{+}-amino acids at 41 °C (20 mmHg). The proximity contour (gray dotted line) denotes the dotted outline that surrounds the ligand, representing the distance to the active site. Ligand solvent exposure is exposed by the blue mark that is drawn behind of the ligand atoms. Solvent exposure of the receptor is evidenced by the turquoise discs drawn behind the residues to indicate the difference in solvent exposure due to the presence of the ligand. The yellow circle with no ring color represents polar amino acids, with red ring symbolize acidic amino acid and with blue ring, basic amino acids. The purple line represents metal contact and the cream-colored dotted line, the solvent contact.

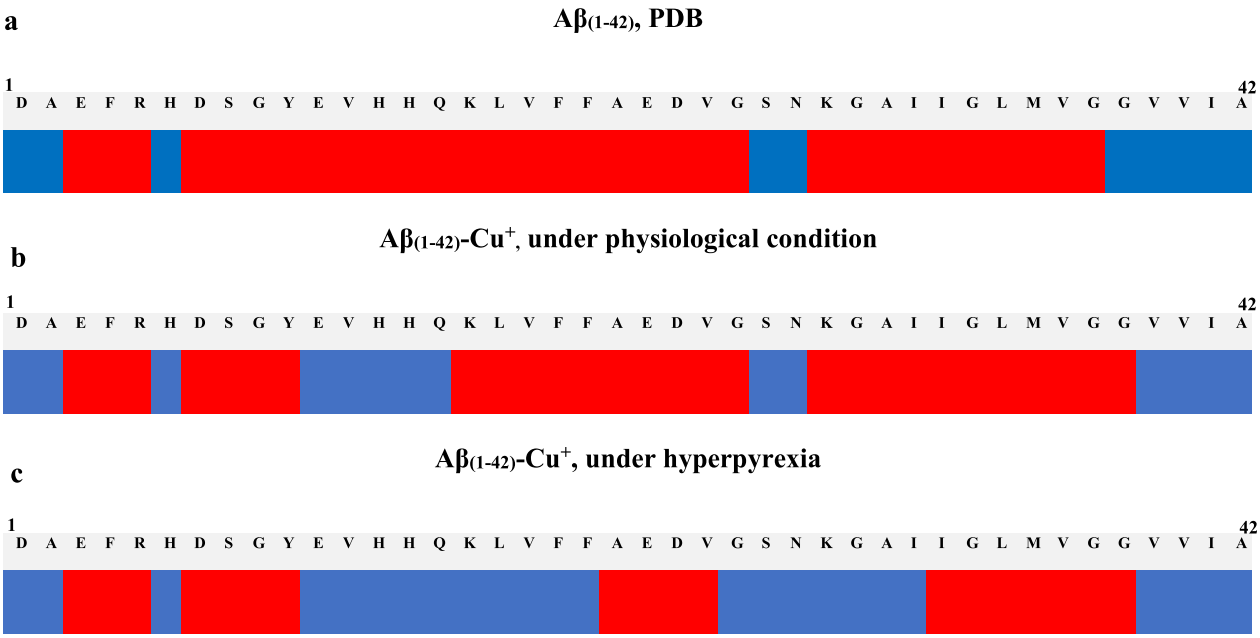

Fig. 4. (**a**) The $A\beta_{(1-42)}$ structure; (**b**) $A\beta_{(1-42)}$-Cu^{+} complex conditioned by the dynamic parameters (heat time of 200 ps at 310.15 K and 1.466 kPa); (**c**) $A\beta_{(1-42)}$-Cu^{+} complex conditioned by the dynamic parameters (heat time of 200 ps at 314.15 K and 2.666 kPa). The system was monitored with a time step of 0.0005 ps, where red represents the α-helix motif and blue, β-sheet.

Table 1
The bond lengths (in Å) between the Cu^{+} ion and the coordination atom from the amino acid involved in the binding process, where in bold are the increased lengths and in italics the short distances according to the molecular dynamics.

Chain	Figure	Nr.	Amino acid residue binding site	37 °C (11 mmHg)	41 °C (20 mmHg)
	$A\beta_{(1-42)}$ – Cu^{+} distance (Å)				
1	2, F & G	1	Glu^{11}(O)	1.74	*1.72*
		2	Tyr^{10}(O)	2.18	**2.22**
		3	Arene π-Contacts	3.00	*2,97*
	$A\beta_{(1-42)}$F – Cu^{+} distance (Å)				
1	5, C1 & D1	1	Tyr^{10}(O)	2.53	*2.52*
		2	Tyr^{10}(O)	2.24	**2.40**
2	5, E1 & F1	1	His^{14}(N)	2.30	*2.29*
		2	His^{14}(N)	2.20	**2.24**
		3	His^{13}(O)	2.43	**2.50**
		4	Val^{12}(O)	2.17	**2.19**
3	5, G1 & H1	1	His^{14}(N)	2.28	*2.22*
		2	His^{14}(N)	2.35	*2.30*
		3	His^{13}(O)	2.27	**2.31**
		4	Val^{12}(O)	2.20	**2.28**
4	5, I1 & J1	1	His^{13}(N)	2.43	**2.50**
		2	His^{13}(O)	2.32	*2.27*
		3	Gln^{15}(O)	2.44	*2.31*
5	5, K1 & L1	1	His^{13}(N)	2.54	*2.45*
		2	Gln^{15}(O)	2.28	*2.26*
		3	His^{13}(O)	–	*2.45*
6	5, M1 & N1	1	Val^{12}(O)	2.47	*2.33*
7	5, O1 & P1	1	His^{14}(N)	2.48	**2.50**
		2	Val^{12}(O)	2.20	**2.21**
8	5, Q1 & R1	1	Tyr^{10}(O)	2.42	*2.32*
9	5, S1 & T1	1	Tyr^{10}(O)	2.65	**2.67**
		2	Tyr^{10}(O)	2.29	**–**

values become more disperse suggesting a random coil structure potentiation of Aβ fibers. This confirms the hypothesis that elevated temperature and higher pressure inhibit the α-helix motif, with direct consequences on the Aβ peptide aggregation.

4. Discussion

Studies have shown that accumulation of metal ions in the brain is closely related to the progression of AD (Wang et al., 2020). Therefore, it is crucial to comprehend the processes underlying the interaction between metal ions and Aβ peptides.

As other studies have shown, hyperpyrexia can negatively influence the neurodegeneration development (Czepiel et al., 2020; Singhal et al., 2020).

In this study, a theoretical comparative analysis of the structural changes of $A\beta_{(1-42)}$ peptide in complexation with different metal ions was performed. We observed that the addition of trace metals considerably accelerates the Aβ aggregation, which may

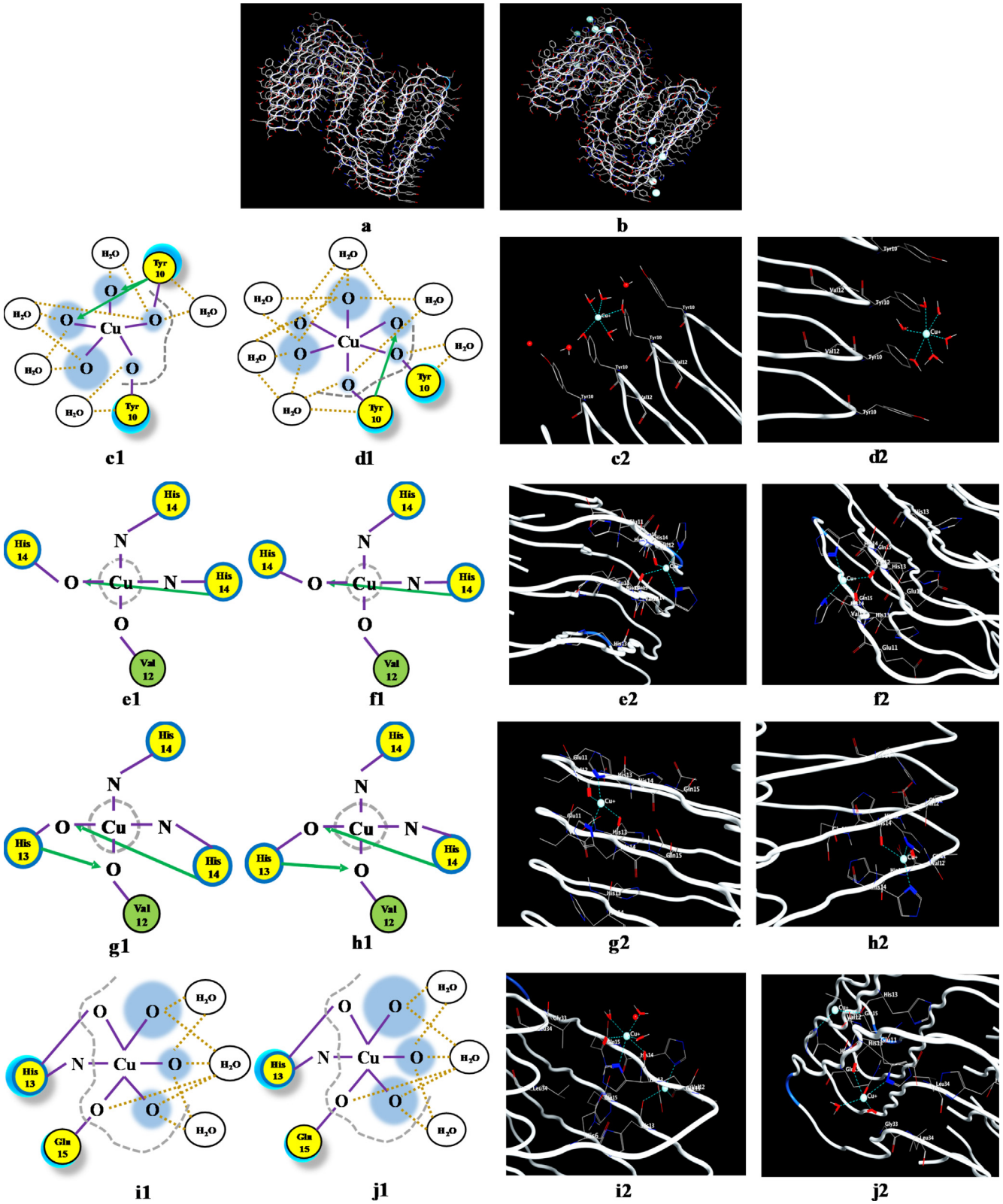

Fig. 5. The effect of temperature and pressure on the $A\beta_{(1\text{-}42)}$F-Cu^{+} complex conformation, highlighted by the use of the molecular dynamics protocol, where: (**a**) $A\beta_{(1\text{-}42)}$F structure and (**b**) $A\beta_{(1\text{-}42)}$F-Cu^{+} structure. Coordination pattern and binding site of $A\beta_{(1\text{-}42)}$F-Cu^{+} at (**c**) 37 °C (11 mmHg) and (**d**) 41 °C (20 mmHg) for Chain 1; (**e**) 37 °C (11 mmHg) and (**f**) 41 °C (20 mmHg) for Chain 2; (**g**) 37 °C (11 mmHg) and (**h**) 41 °C (20 mmHg) for Chain 3; (**i**) 37 °C (11 mmHg) and (**j**) 41 °C (20 mmHg) for Chain 4; (**k**) 37 °C (11 mmHg) and (**l**) 41 °C (20 mmHg) for Chain 5; (**m**) 37 °C (11 mmHg) and (**n**) 41 °C (20 mmHg) for Chain 6; (**o**) 37 °C (11 mmHg) and (**p**) 41 °C (20 mmHg) for Chain 7; (**q**) 37 °C (11 mmHg) and (**r**) 41 °C (20 mmHg) for Chain 8; (**s**) 37 °C (11 mmHg) and (**t**) 41 °C (20 mmHg) for Chain 9. The green circle represents the amino acids with no polar or charged side chain.

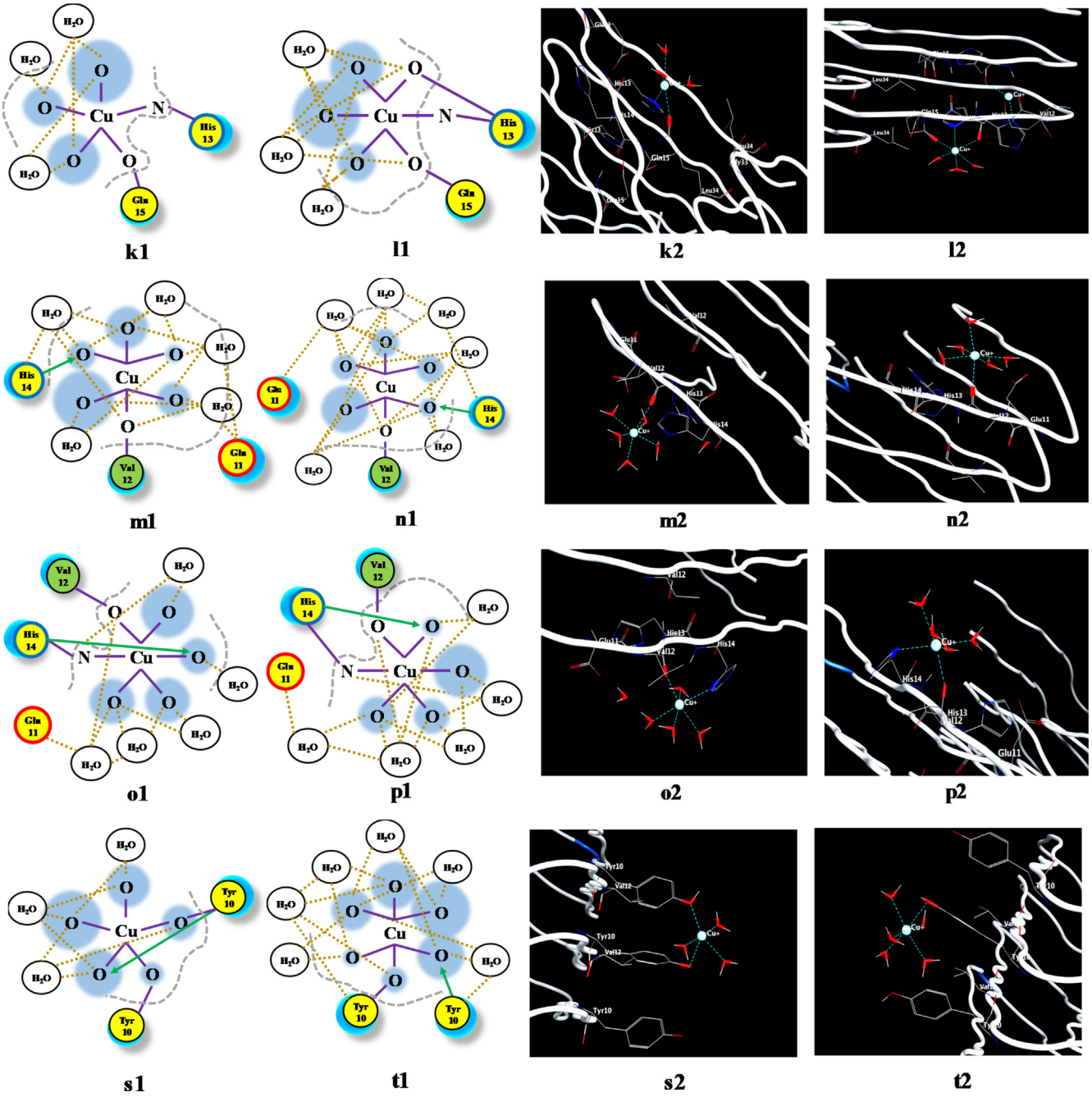

Fig. 5 (*continued*)

contribute to neurotoxicity (Hane and Leonenko, 2014). Hence, the *in silico* experiments were based on the Aβ conformational differences, under normal physiological conditions compared to hyperpyretic pathophysiological effects.

Our data suggest that there are major differences in the structure of amyloid beta peptides under elevated temperature and pressure. The interaction between metal ions and Aβ peptides is maximized at the beginning of the simulations and stabilizes when the temperature becomes constant (Boopathi and Kolandaivel, 2014). Furthermore, the copper ion plays an important role in conformational changes of Aβ peptides by increasing or decreasing the intramolecular distances within the AD fibrils. Moreover, according to the Madisen investigations, Cu is released as well yielding micromolar concentrations in specific synaptic clefts (Madsen and Gitlin, 2007). In addition, these ions have been shown to form an intramolecular complex with amyloid-beta peptides due to substoichiometric levels used in kinetic investigations (Sarell et al., 2010). All these factors lead to serious complications in both hyperpyrexia and Alzheimer's patients. It has been observed that both elevated temperature and high intracranial pressure accentuate the aggregation process, by transforming the α-helix into the β-sheet conformation and random coil motif. These molecular simulation data suggest that, for amyloid beta monomer, the 1–16 region has a higher binding potential In the case of amyloid beta fibrils ($A\beta_{(1\text{-}42)}F$), the metal ions binding potential increases even in the 17–42C-terminal region. These conformations (β-sheet and random coil structure) increase the aggregation processes by promoting the formation of new intermolecular hydrogen bonds

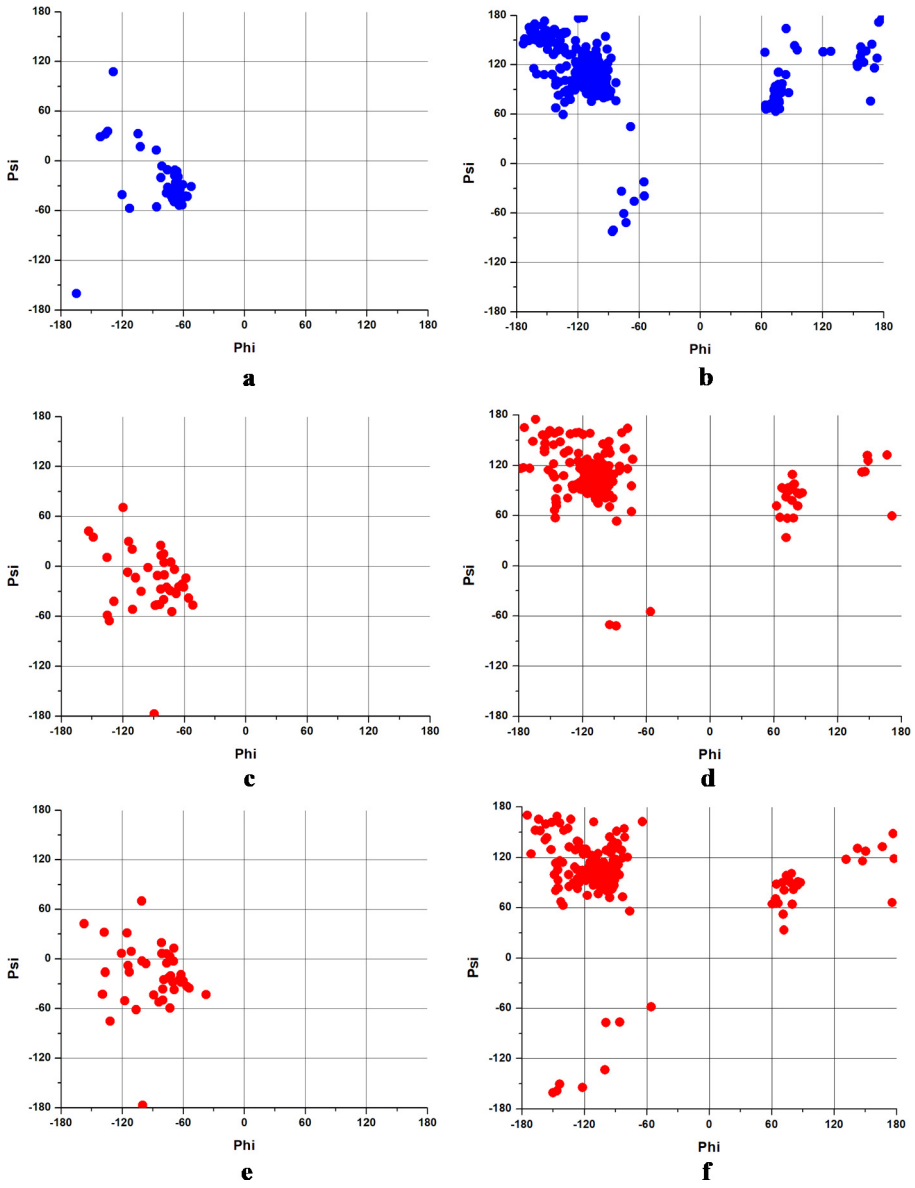

Fig. 6. The Ramachandran plot of (**a**) $A\beta_{(1-42)}$ (PDB), (**b**) $A\beta_{(1-42)}F$ (PDB), (**c**) $A\beta_{(1-42)}$ at 37 °C and 11 mmHg, (**d**)$A\beta_{(1-42)}F$ at 37 °C and 11 mmHg, (**e**)$A\beta_{(1-42)}$ at 41 °C and 20 mmHg and (**f**) $A\beta_{(1-42)}F$ at 41 °C and 20 mmHg.

between monomeric forms of $A\beta_{(1-42)}$. Therefore, a higher temperature and ICP can intensify the processes of peptide aggregation at the cortical level, with direct consequences on the morphology of the AD brain. In addition, these results could be explained by the metal-binding kinetics parameters. According to the Pedersen and Noy, the association of Cu ions seems to be very fast and likely close to diffusion controlled (Pedersen et al, 2012; Noy et al, 2008). Copper ion can rapidly exchange with others metal ions and hence, due to the system dynamics and heat friction, the temperature may rise by association and dissociation reactions (Faller et al, 2014). Moreover, according to recent publications, copper ions alter Aβ kinetics, guiding its aggregation from a more stable fibrillar structure, to a pathway that leads to neurotoxic aggregates (Hane and Leonenko, 2014).

In the case of Aβ(1–42), a significant modification occurred in structure conformation due to the decrease of α-helix population to the advantage of β-sheet structure formation, while for β-amyloid fibrils, lack of α-helix structure. These noteworthy changes can be studied in terms of binding sites and interaction between Cu^{+} ions and the corresponding Aβ residues. Moreover, according to these results, tyrosine plays an important role in coordination stabilizations. This feature was also observed by, using DFT calculations which provided a mechanism that included Tyr^{10} as a key component in mutagenesis tests (Barnham et al., 2004). Furthermore, the same implications were also noticed which demonstrated that the presence of Tyr in the primary structure of amyloid-beta regulates the formation of toxic β-sheets (Coskuner and Uversky, 2017). In addition, a study from 2019 showed that the structural models obtained with an extended statistical method displays Tys-Tys and Cu-carboxylate interactions are enhanced in dimers (La Penna et al., 2019). Besides, tyrosine oxidation could interfere in metal complexation with copper due to the quinoline generation (Mocanu et al., 2020). Therefore, under these circumstances, the copper ion may form chemical bonds between different beta-amyloid oligomers that could enhance fibril formation.

Following the application of dynamic conditions, no significant differences were observed regarding $A\beta_{(1-42)}$ structure using physiological AD and hyperpyretic conditions. Regarding $A\beta_{(1-42)}F$ structure, the same buildup predisposition is noticed in the β-sheet area in both simulations. These findings support the hypothesis that a higher temperature and elevated pressure impair the α-helix structure, with direct consequences in peptide aggregation. Furthermore, a recent study proved that that the high dynamics of the metal-peptide interaction is incompatible with high control of the metal ions reactivity (Faller et al, 2014). Hence, according to this argument and to our results, the hyperpyretic conditions and the amyloid-beta cascade could enhance the AD pathological symptoms by promoting a extrinsic energy of Cu- Aβ interactions.

Moreover, our results confirmed the molecular pathway in which the copper was involved in amyloid-beta interactions. According to Marino, the DFT computational study showed that cooper ion possesses a predisposition to penta-coordination (Marino et al., 2010). In addition, evidence for the involvement of histidine residues of beta-amyloid peptides as N-ligands has been supported by investigations on the complexes formed.

In this study, we demonstrated that the peptide aggregation process may increase due to the promotion of β-sheet and random coil secondary conformations. However, However, for full confirmation of the hypothesis advanced here, further studies should be carried out to determine the structure, interaction and function of the peptide under the action of metal ions.

5. Conclusions

Our findings support the hypothesis that a higher temperature and elevated pressure impair the α-helix structure, with direct consequences on peptide aggregation. Furthermore, the molecular dynamics data show that these conditions may increase the peptide aggregation process due to the formation of β-sheet and random coil secondary conformations. Moreover, the presence of metal ions in the cortical areas of AD brain caused by abnormal metabolism can have a negative effect over the neurodegeneration rate.

Considering both diseased conditions (AD and hyperpyrexia) further experimental approaches, such as SDS-PAGE with a time and temperature dependent incubation of amyloid-beta 1–42 peptide, AFM, SEM, *in vivo* investigations of AD model of cells culture, will be applied to extend our current findings to other studies with relevance for developing new efficient treatment strategies.

Author's contributions

Conceptualization, C.S.M.; methodology, C.S.M. and L.I.; software, C.S.M.; validation, C.S.M. and G.D.; formal analysis, C.S.M. and G.D.; investigation, C.S.M; resources C.S.M.; data curation, C. S.M., L.I. and G.D.; writing—original draft preparation, C.S.M.; writing—review and editing, C.S.M., L.I., B.A.P., V.R.G. and G.D.; visualization, C.S.M., L.I. and G.D.; supervision, G.D.; project administration, C.S.M., V.R.G. and G.D. All authors have read and agreed to the published version of the manuscript.

Informed consent statement

Not applicable.

Disclosure of any conflicts of interest.

The authors declare no conflict of interest. The funders had no role in the design of the study; in the collection, analyses, or interpretation of data; in the writing of the manuscript, or in the decision to publish the results.

Funding.

The authors wish to thank the financial support from the Romanian Government through UEFISCDI Bucharest (PN-III-P2-2.1-PED2019-2484, Contract PED494, BioPASCAL).

CRediT authorship contribution statement

Cosmin Stefan Mocanu: Conceptualization, Methodology, Software, Validation, Formal analysis, Investigation, Resources, Data curation, Writing – original draft, Writing – review & editing, Visualization, Project administration. **Laura Darie-Ion:** Methodology, Data curation, Writing – review & editing, Visualization. **Brindusa Alina Petre:** Writing – review & editing. **Vasile Robert Gradinaru:** Writing – review & editing, Project administration. **Gabi Drochioiu:** Validation, Formal analysis, Data curation, Writing – review & editing, Visualization, Supervision, Project administration.

Declaration of Competing Interest

The authors declare that they have no known competing financial interests or personal relationships that could have appeared to influence the work reported in this paper.

References

Allahdadi, K.J., Walker, B.R., Kanagy, N.L., 2005. Augmented endothelin vasoconstriction in intermittent hypoxia-induced hypertension. Hypertension 45, 705–709. https://doi.org/10.1161/01.HYP.0000153794.52852.04.

Europe, A., 2020. Data sharing in dementia research – the EU landscape; Publisher: Gates Ventures. Luxembourg, Luxembourg, pp. 3–25.

Alzheimer's Association 2020. Alzheimer's disease facts and figures. Alzheimer Dement. 16, 391-460. https://doi.org/10.1002/alz.12068.

Barnham, K.J., Haeffner, F., Giccotosto, G.D., Curtain, C.C., Tew, D., Mavros, C., Beyreuther, K., Carrington, D., Masters, C.L., Cherny, R.A., Cappai, R., Bush, A.I., 2004. Tyrosine gated electron transfer is key to the toxic mechanism of Alzheimer's disease β-amyloid. FASEB J 18, 1427–1429. https://doi.org/10.1096/fj.04-1890fje.

Bieschke, J., Herbst, M., Wiglenda, T., Friedrich, R.P., Boeddrich, A., Schiele, F., Kleckers, D., Lopez del Amo, J.M., Grüning, B.A., Wang, Q., Schmidt, M.R., Lurz, R., Anwyl, R., Schnoegl, S., Fändrich, M., Frank, R.F., Reif, B., Günther, S., Walsh, D.M., Wanker, E.E., 2012. Small-molecule conversion of toxic oligomers to nontoxic β-sheet-rich amyloid fibrils. Nat. Chem. Biol. 8 (1), 93–101.

Bond, S.D., Leimkuhler, B.J., Laird, B.B., 1999. The Nosé-Poincaré method for constant temperature molecular dynamics. J. Comp. Phys. 151, 114–134. https://doi.org/10.1006/jcph.1998.6171.

Boopathi, S., Kolandaivel, P., 2014. Role of zinc and copper metal ions in amyloid β-peptides Aβ 1–40 and Aβ1–42 aggregation. RSC Adv. 4, 38951–38965. https://doi.org/10.1039/C4RA05390G.

Coskuner, O., Uversky, V.N., 2017. Tyrosine regulates β-sheet structure formation in Amyloid-β42: a new clustering algorithm for disordered proteins. J. Chem. Inf. Mod. 57, 1342–1358. https://doi.org/10.1021/acs.jcim.6b00761.

Crescenzi, O., Tomaselli, S., Guerrini, R., Salvadori, S., D'Ursi, A., Temussi, A., Picone, D., 2002. Solution structure of the Alzheimer amyloid β-peptide (1–42) in an apolar microenvironment. European Journal of Biochemistry 269 (22), 5642–5648. https://doi.org/10.1046/j.1432-1033.2002.03271.x. In press.

Czepiel, K.S., Lucas, A.T., Whalen, M.J., Mojica, J.E., 2020. Dexmedetomidine-associated hyperpyrexia in three critically ill patients with coronavirus disease 2019. Crit. Care Explorations 2. https://doi.org/10.1097/CCE.0000000000000213.

Faller, P., Hureau, C., Berthoumieu, O., 2013. Role of metal ions in the self-assembly of the Alzheimer's amyloid-β peptide. Inorg. Chem. 52, 12193–12206. https://doi.org/10.1021/ic4003059.

Faller, P., Hureau, C., La Penna, G., 2014. Metal ions and intrinsically disordered proteins and peptides: from Cu/Zn amyloid-β to general principles. Acc. Chem. Res. 47, 2252–2259. https://doi.org/10.1021/ar400293h.

Fan, L., Mao, C., Hu, X., Zhang, S., Yang, Z., Hu, Z., Sun, H., Fan, Y.u., Dong, Y., Yang, J., Shi, C., Xu, Y., 2020. New insights into the pathogenesis of Alzheimer's disease. Front. Neurol. 10. https://doi.org/10.3389/fneur.2019.01312.

Ghajar, J., 2000. Traumatic brain injury. Lancet 356, 923–929. https://doi.org/10.1016/S0140-6736(00)02689-1.

Gremer, L., Schölzel, D., Schenk, C., Reinartz, E., Labahn, J., Ravelli, R.B.G., Tusche, M., Lopez-Iglesias, C., Hoyer, W., Heise, H., Willbold, D., Schröder, G.F., 2017. Fibril structure of amyloid-β (1–42) by cryo–electron microscopy. Science 358 (6359), 116–119.

Guo, T., Zhang, D., Zeng, Y., Huang, T.Y., Xu, H., Zhao, Y., 2020. Molecular and cellular mechanisms underlying the pathogenesis of Alzheimer's disease. Mol. Neurodegener. 15, 1–37. https://doi.org/10.1186/s13024-020-00391-7.

Halgren, T.A., 1996. Merck molecular force field. I. Basis, form, scope, parameterization, and performance of MMFF94. J. Comp. Chem. 17, 490–519. https://doi.org/10.1002/(SICI)1096-987X(199604)17:5/6<490::AID-JCC1>3.0.CO;2-P.

Hane, F., Leonenko, Z., 2014. Effect of metals on kinetic pathways of amyloid-β aggregation. Biomolecules. 4, 101–116. https://doi.org/10.3390/biom4010101.

Huang, X., Cuajungco, M.P., Atwood, C.S., Hartshorn, M.A., Tyndall, J.D.A., Hanson, G. R., Stokes, K.C., Leopold, M., Multhaup, G., Goldstein, L.E., Scarpa, R.C., Saunders, A.J., Lim, J., Moir, R.D., Glabe, C., Bowden, E.F., Masters, C.L., Fairlie, D.P., Tanzi, R. E., Bush, A.I., 1999. Cu(II) potentiation of Alzheimer Aβ neurotoxicity: Correlation with cell-free hydrogen peroxide production and metal reduction. J. Biol. Chem. 274 (52), 37111–37116.

G. La Penna Li., M.S., Computational models explain how copper binding to amyloid-β peptide oligomers enhance oxidative pathways Phys. Chem. Chem. Phys. 21 2019 8774 10.1039/C9CP00293F.

Lin, Y.F., Cheng, C.W., Shih, C.S., Hwang, J.K., Yu, C.S., Lu, C.H., 2016. MIB: metal ion-binding site prediction and docking server. J. Chem. Inf. Model. 56, 2287–2291. https://doi.org/10.1021/acs.jcim.6b00407.

Liu, D., Fu, D., Zhang, L., Sun, L., 2021. Detection of amyloid-beta by Fmoc-KLVFF self-assembled fluorescent nanoparticles for Alzheimer's disease diagnosis. Chin. Chem. Lett. 32, 1066–1070. https://doi.org/10.1016/j.cclet.2020.09.009.

Lu, C.-H., Lin, Y.-F., Lin, J.-J., Yu, C.-S., Vertessy, B.G., 2012. Prediction of metal ion–binding sites in proteins using the fragment transformation method. PloS one 7 (6), e39252.

Luhrs, T., Rotter, C., Adrian, M., Riek-Loher, D., Bohrmann, B., Dobeli, H., 2005. 3D structure of Alzheimer's amyloid-beta(1–42) fibrils. Proc. Natl. Acad. Sci. USA 102, 17342–17347. https://doi.org/10.1073/pnas.0506723102.

Lupaescu, A.V., Mocanu, C.S., Drochioiu, G., Ciobanu, C.I., 2021. Zinc binding to NAP-type neuroprotective peptides: nuclear magnetic resonance studies and molecular modeling. Pharmaceuticals. 14, 1011. https://doi.org/10.3390/ph14101011.

Madsen, E., Gitlin, J.D., 2007. Copper and iron disorders of the brain. Annu. Rev. Neurosci. 30, 317–337. https://doi.org/10.1146/annurev.neuro.30.051606.094232.

Marino, T., Russo, N., Toscano, M., Pavelka, M., 2010. On the metal ion (Zn^{2+}, Cu^{2+}) coordination with beta-amyloid peptide: DFT computational study. Interdiscip. Sci. Comput. Life Sci. 2, 57–69. https://doi.org/10.1007/s12539-010-0086-x.

Markesbury, W., Lovell, M., 2007. Damage to lipids, proteins, DNA and RNA in mild cognative impairment. Arch. Neurol. 64, 954–956. https://doi.org/10.1001/archneur.64.7.954.

Makin, O.S., Atkins, E., Sikorski, P., Johansson, J., Serpell, L., 2005. Molecular basis for amyloid fibril formation and stability. Proc. Natl. Acad. Sci. USA 102, 315–320. https://doi.org/10.1073/pnas.0406847102.

Mocanu, C.S., Drochioiu, G., 2021. The Interaction of Possible Anti-AD ASA-NAP Peptide Conjugate with Tubulin: A Theoretical and Experimental Insight. Int. J. Pept. Res. Ther. 27 (4), 2487–2503.

Mocanu, C.S., Jureschi, M., Drochioiu, G., 2020. Aluminium binding to modified amyloid-β peptides: implications for Alzheimer's disease. Molecules 25, 4536. https://doi.org/10.3390/molecules25194536.

Mocanu, C.S., Petre, B.A., Darie-Ion, L., Drochioiu, G., Niculaua, M., Stoica, I., Homocianu, M., Nita, L.E., Gradinaru, V.R., 2022. Structural characterization of a new collagen biomimetic octapeptide with nanoscale self-assembly potential: experimental and theoretical approaches. ChemPlusChem e202100462. 87 (2). https://doi.org/10.1002/cplu.202100462.

Molecular Operating Environment (MOE) (2013.08), Montreal, QC, Canada: Chemical Computing Group Inc 2017.

Mukandala, G., Tynan, R., Lanigan, S., O'Connor, J.J., 2016. The effects of hypoxia and inflammation on synaptic signaling in the CNS. Brain. Sci. 6, 6 https://doi:10.3390/brainsci6010006.

R.Y. Noa B. Shiri I. Abu-Kishk B. Meirav S. Ruth K. Eran Correction to: Hyperpyrexia and high fever as a predictor for serious bacterial infection (SBI) in children—a systematic review Eur. J. Pediatr. 179 2020 353 353 10.1007/s00431-019-03525-2.

Noy, D., Solomonov, I., Sinkevich, O., Arad, T., Kjaer, K., Sagi, I., 2008. Zinc−amyloid β interactions on a millisecond time-scale stabilize non-fibrillar Alzheimer-related species. J. Am. Chem. Soc. 130, 1376–1383. https://doi.org/10.1021/ja076282l.

Pedersen, J.T., Hureau, C., Hemmingsen, L., Heegaard, N.H., Ostergaard, J., Vasak, M., Faller, P., 2012. Rapid exchange of metal between Zn 7-metallothionein-3 and amyloid-β peptide promotes amyloid related structural changes. Biochem. 51, 1697–1706. https://doi.org/10.1021/bi201774z.

Pedersen, J.T., Østergaard, J., Rozlosnik, N., Gammelgaard, B., Heegaard, N.H.H., 2011. Cu(II) mediates kinetically distinct, non-amyloidogenic aggregation of amyloid-beta peptides. J. Biol. Chem. 286, 26952–26963. https://doi.org/10.1074/jbc.M111.220863.

Sarell, C.J., Wilkinson, S.R., Viles, J.H., 2010. Substoichiometric levels of Cu^{2+} ions accelerate the kinetics of fiber formation and promote cell toxicity of amyloid-beta from Alzheimer disease. J. Biol. Chem. 285, 41533–41540. https://doi.org/10.1074/jbc.M110.171355.

Sciacca, M.F., Di Natale, G., Tosto, R., Milardi, D., Pappalardo, G., 2020. Tau/Aβ chimera peptides: Evaluating the dual function of metal coordination and membrane interaction in one sequence. J. Inorg. Biochem. 205,. https://doi.org/10.1016/j.jinorgbio.2020.110996 110996.

Serrano-Pozo, A., Frosch, M.P., Masliah, E., Hyman, B.T., 2011. Neuropathological alterations in Alzheimer disease. Cold. Spring. Harb. Perspect. Med. 1, https://doi:10.1101/cshperspect.a006189 a006189.

T. Singhal S. Phadtare S. Pai A. Raodeo Hyperpyrexia leading to death in a patient with severe COVID-19 disease. medRxiv 2020 10.1101/2020.05.18.20097220.

Stretti, F., Gotti, M., Pifferi, S., Brandi, G., Annoni, F., Stocchetti, N., 2014. Body temperature affects cerebral hemodynamics in acutely brain injured patients: an observational transcranial color-coded duplex sonography study. Crit. Care. 18, 1–7. https://doi.org/10.1186/s13054-014-0552-7.

Strodel, B., Coskuner-Weber, O., 2019. Transition metal ion interactions with disordered amyloid-β peptides in the pathogenesis of Alzheimer disease: Insights from computational chemistry studies. J. Chem. Inf. Model. 59, 1782–1805. https://doi.org/10.1021/acs.jcim.8b00983.

Sturgeon, J.B., Laird, B.B., 2000. Symplectic algorithm for constant-pressure molecular dynamics using a Nosé-Poincaré thermostat. J. Chem. Phys. 112, 3474–3482. https://doi.org/10.1063/1.480502.

Tambini, M.D., Norris, K.A., D'Adamio, L., 2020. Opposite changes in APP processing and human Aβ levels in rats carrying either a protective or a pathogenic APP mutation. Elife 9, e52612.

Vijayan, D., Chandra, R., 2020. Amyloid beta hypothesis in Alzheimer's disease: major culprits and recent therapeutic strategies. Curr. Drug. Targets. 21, 148–166. https://doi.org/10.2174/1389450120666190806153206.

Von Bergen, M., Friedhoff, P., Biernat, J., Heberle, J., Mandelkow, E.M., Mandelkow, E., 2000. Assembly of τ protein into Alzheimer paired helical filaments depends on a local sequence motif (306VQIVYK311) forming β structure. Proc. Natl. Acad. Sci. 97, 5129–5134. https://doi.org/10.1073/pnas.97.10.5129.

Wang, L., Yin, Y.L., Liu, X.Z., Shen, P., Zheng, Y.G., Lan, X.R., Lu, C.B., Wang, J.Z., 2020. Current understanding of metal ions in the pathogenesis of Alzheimer's disease. Transl. Neurodegener. 9, 1–13. https://doi.org/10.1186/s40035-020-00189-z.

Weuve, J., Hebert, L.E., Scherr, P.A., Evans, D.A., 2014. Deaths in the United States among persons with Alzheimer's disease (2010–2050). Alzheimer. Dement. 10, e40–e46. https://doi.org/10.1016/j.jalz.2014.01.004.